Detailed physicochemical and thermochemical investigation of Upper Assam oil shale

Bhargav Baruah[1] · Rupam Kataki[2] · Parash Thakur[3] · Pankaj Tiwari[1]

Abstract

The present work provides a detailed characterization and kinetic study of oil shale of Upper Assam, India. The physicochemical characteristics of oil shale were studied by proximate analysis, elemental analysis, Fourier transform infrared spectroscopy and X-ray diffraction. The physicochemical study showed the oil shale to be of siliceous type, sour in the presence of aliphatic, aromatic and phenolic compounds. The thermal decomposition of the oil shale was studied using thermogravimetric analysis at heating rates of 10, 20, 30 and 50 °C min^{-1}. The kinetic study of oil shale pyrolysis process was performed on the thermogravimetric data using three model-free isoconversional methods, viz. Friedman, Flynn–Wall–Ozawa and Kissinger–Akahira–Sunose. The reaction mechanisms were determined using the Criado master plot. The understanding of the composition of Indian oil shale and pyrolysis process kinetics can help establishing the experimental parameters for the extraction of valuable products from the oil shale.

Keywords Upper Assam oil shale · Physicochemical properties · Thermochemical properties · Model-free isoconversional methods · Criado master plot

Abbreviations

AC	Ash content
DTG	Differential thermogravimetry
FC	Fixed carbon
FTIR	Fourier transform infrared spectroscopy
FWO	Flynn–Wall–Ozawa
KAS	Kissinger–Akahira–Sunose
MC	Moisture content
TOC	Total organic carbon
TG	Thermogravimetric analysis
VM	Volatile matter
XRD	X-ray diffraction

Symbols

A	Pre-exponential factor (s^{-1})
C	Carbon
E	Activation energy (kJ mol^{-1})
$f(\alpha)$	Reaction mechanism
$g(\alpha)$	Integral form of reaction mechanism
H	Hydrogen
$k(T)$ or k	Reaction rate constant (s^{-1})
N	Nitrogen
R	Gas constant (8.314 J mol^{-1} K^{-1})
S	Sulfur
T	Absolute temperature (K)
w_o	Initial mass
w_T	Mass at temperature, T
w_α	Mass at conversion, α
t	Conversion time (s)
α	Conversion degree
β	Heating rate (°C min^{-1})

✉ Rupam Kataki
rupam@tezu.ernet.in

✉ Pankaj Tiwari
pankaj.tiwari@iitg.ernet.in

1 Department of Chemical Engineering, Indian Institute of Technology Guwahati, Guwahati, Assam 781039, India

2 Department of Energy, Tezpur University, Tezpur, Assam 784028, India

3 Oil India Limited, Duliajan, Assam 786602, India

Introduction

With the depletion of petroleum reservoirs, the unconventional petroleum reserves are gaining importance. One such unconventional petroleum reserve is oil shale, which has emerged as a promising and viable substitute to conventional petroleum [1]. Oil shale is a finely grained, porous, sedimentary rock which contains organic matter known as kerogen, concealed inside a mineral matrix [2]. Kerogen is a complex organic compound which acts as the source of production of both conventional and unconventional petroleum and natural gases. On the application of heat, kerogen converts into bitumen which further breaks down into oil and gas [2, 3]. The most common and suitable method for the production of oil and gas from oil shales is retorting or pyrolysis [3–8]. The pyrolysis procedure of oil shale decomposition is affected by various factors such as heating rate, pyrolysis temperature, holding time, particle size, mineral matters present in oil shale and type of reactor used for pyrolysis [4–6, 9, 10]. Oil shales are classified based on the minerals present, type of kerogen, age of deposition and source origin. Based on mineral matters and aesthetics, oil shales are generally classified into three types, viz. carbonate shale, siliceous shale and cannel coal [11–13]. The mineral matters present in oil shale plays a significant role in retorting or pyrolysis of oil shale. Silica, carbonate, pyrite, etc. can drastically govern the heat transfer in oil shale and influence the composition of products formed during pyrolysis of oil shale. [14–16]. The thermal decomposition of oil shale requires very high temperature. Decomposition of organic matter generally transpires from about 200–600 °C and the mineral matters start to decompose from about 600 °C [17–19]. The decomposition of organic matter in oil shales is a complex process, and the kinetic parameters of different oil shales have been extensively studied. Previously, the pyrolysis process of decomposition of different oil shales has been explained through two consecutive first-order reactions [20–23]. The decomposition of Moroccan oil shale and its kerogen has been determined using model fitting and model-free methods and reported the oil shale to follow diffusion mechanism (D4) [24]. The study of the demineralization of Jordanian oil shale showed catalytic and inhibition behavior of the minerals present in oil shale [25]. Further, advanced isoconversional method has also been reported for the determination of oil shale pyrolysis kinetics [17, 26].

Upper Assam oil shale reserves are estimated to be over 15 billion barrels [27], are found along the coal mines of Barail formation, Northeast India, and belong to the Tertiary period. These oil shales are considered to be the source rocks for the petroleum reserve of Upper Assam region [11, 27]. Oil shales occur as out crops and over burden to the coal seams of the Northeastern Coal Fields and are dumped by Coal India Limited in designated dumping sites. No study has been reported on the kinetic study of the pyrolysis of Indian oil shale. The present work aims to produce a complete physicochemical and thermochemical analysis of Indian oil shale and provide a comprehensive kinetic analysis of the pyrolysis process. The understanding of the composition of Indian oil shale and pyrolysis process kinetics can help establishing the experimental parameters for the extraction of pyrolytic oil, gas and char from the oil shale.

Materials and methodology

Materials

Oil shale samples were collected from the East mine of the Tikak Colliery, Makum Coal Fields, Margherita (Tinsukia District), Upper Assam, India. The samples were collected directly from the mine and thus were not processed prior to collection. The oil shale samples have a brown to dark brown texture with black streamlines appearing on the surface. The samples were ground using a mechanical crusher and screened to 100 mesh size (150 microns).

Ultimate analysis, proximate analysis and total organic carbon (TOC)

The ultimate analysis (carbon, hydrogen, nitrogen, sulfur) of oil shale samples was performed using a EuroVector EA3000 Elemental Analyzer. The analysis was performed with a linear calibration. The proximate analysis of oil shale samples was performed according to ASTM D 3173, ASTM D 3174 and ASTM D 3175 methods [28]. The fixed carbon was determined by difference [FC = 100 − (VM + AC + MC)], where FC = fixed carbon; VM = volatile matter; AC = ash content; MC = moisture content. The fixed carbon was calculated on dry basis. The total organic carbon was evaluated using Walkley–Black titration method [29].

Fourier transform infrared spectrometry and X-ray diffraction

FTIR analysis was performed to determine the functional groups present in oil shale using PerkinElmer FTIR spectrometer Frontier. The powdered samples were mixed with KBr powder to make pellets for the analysis. The wave number (cm^{-1}) was set from 400 to 4200 cm^{-1}.

X-ray diffraction analysis was performed to identify the different mineral matters present in the oil shale using a Bruker D8 Advance XRD instrument. The 2θ values were

Table 1 Isoconversional methods considered for kinetic analysis

Isoconversional methods	Methods	Expressions	Comments
Differential	Friedman	$\ln\left(\frac{d\alpha}{dt}\right) = \ln\left(\beta\frac{d\alpha}{dT_\alpha}\right) = \ln[Af(\alpha)] - \frac{E_a}{RT_\alpha}$	Friedman method is a differential isoconversional method, is applicable to multiple heating rate data and is sensitive to small changes in rate data
			For any constant value of α, the effective activation energy can be obtained over a wide range of temperatures by plotting $\ln\left(\beta\frac{d\alpha}{dT}\right)$ versus $\frac{1}{T}$ [34]
Integral	Flynn–Wall–Ozawa (FWO)	$\ln\beta_i = \ln\frac{AE_a}{Rg(x)} - 5.331 - 1.052\frac{E_a}{RT_\alpha}$	FWO method is a modified form of the general isoconversional equation
			$\ln\left(\frac{\beta_i}{T_{\alpha,i}^B}\right) = \text{constant} - C\left(\frac{E_a}{RT_\alpha}\right)$ by using Doyle approximation of $B = 0$, $C = 1.052$
			For any constant value of α, the effective activation energy can be obtained over a wide range of temperatures by plotting lnβ versus $\frac{1}{T}$ [35, 36]
	Kissinger–Akahira–Sunose (KAS)	$\ln\frac{\beta_i}{T_{\alpha,i}^2} = \ln\left(\frac{AR}{E_\alpha g(\alpha)}\right) - \frac{E_a}{RT_\alpha}$	KAS method is a modified form of the general isoconversional equation
			$\ln\left(\frac{\beta_i}{T_{\alpha,i}^B}\right) = \text{constant} - C\left(\frac{E_a}{RT_\alpha}\right)$
			By using Murray and White approximation of $B = 2$, $C = 1$
			Plotting between $\ln\frac{\beta}{T^2}$ versus $\frac{1}{T}$ for any constant value of α will provide the value of effective activation energy [37]

set from 10° to 80°. The scanning rate was set at $1°\text{min}^{-1}$ with a step size of 0.2°. The analysis of the XRD data was performed using MATCH! 3.

Thermogravimetric analysis

Thermogravimetric analysis (TG) was performed using a NETZSCH TG 209F1 Libra analyzer (Germany). Oil shale samples (about 8–10 mg) of 100 mesh size (150 microns) were heated from 30 to 1000 °C, at four different heating rates of 10, 20, 30 and 50 °C min^{-1}, respectively. Nitrogen was used as purge and balance gas at flow rate of 40 mL min^{-1} and 20 mL min^{-1}, respectively. The samples were held at maximum temperature for 10 min.

Kinetic Study

During pyrolysis of oil shale, the organic matter (kerogen) gets converted into to oil, gas, and char. This conversion is caused by breaking of bonds and occurrence of multiple parallel reactions [17].

Kerogen → Bitumen → Oil + Gas + Char

The conversion of kerogen due to the influence of rise in temperature can be better visualized by TG analysis. Kinetic study of the conversion process on the basis of TG data has been extensively reported in the literature [17, 19, 30, 31]. The kinetic study is commonly performed through model fitting and model-free methods [17, 26, 32, 33]. In the present study, organic matter decomposition zone, identified from the TG–DTG curve, has been considered as the pyrolytic zone. The organic decomposition zone has been considered as single decomposition zone. Model-free isoconversional methods have been considered for the kinetic study.

For the conversion of organic matter in TG mass loss data defined by the Arrhenius equation [32, 33], the rate of conversion for non-isothermal condition can be calculated as

$$\beta\frac{d\alpha}{dT} = A\exp\left(\frac{-Ea}{RT}\right)f(\alpha) \tag{1}$$

Model-free isoconversional methods allow to determine the activation energy of any reaction without foregoing assumption of reaction model. The isoconversional methods are based on the isoconversional principle, which states that at constant conversion the reaction rate is a function of temperature [26, 32]. The differential (Friedman) [34] and integral (Flynn–Wall–Ozawa (FWO) [35, 36] and Kissinger–Akahira–Sunose (KAS) [37]) models have been formulated based on different assumptions on the standard isoconversional equation,

Table 2 Characteristics of Upper Assam oil shale and comparison with different oil shales around the world

Oil shales	C/mass%	H/mass%	N/mass%	S/mass%	Moisture/mass%	Ash/mass%	Volatile matter/mass%	Fixed carbon/mass%	TOC/mass%
Upper Assam[a]	30.06	2.80	1.44	3.61	4.43	53.93	31.78	9.86	6.11
Kukersite [45, 51]	27.90	2.90	0.02	0.86 (avg)	1.30	47.88	46.25	4.57	36.40
Green Rive [46, 52, 53]	17.45	1.60	0.53	0.18	0.30	66.80	33.20	0.00	15.80
Colorado [47, 53, 54]	17.50	2.50	0.50	0.60	1.9	61.90	26.90	11.20	10.66
Huadian [18, 55]	29.23	4.28	0.61	4.92	3.26	56.91	39.34	3.75	8.70 (avg)

[a]Tikak Colliery, Makum Coal Field, India
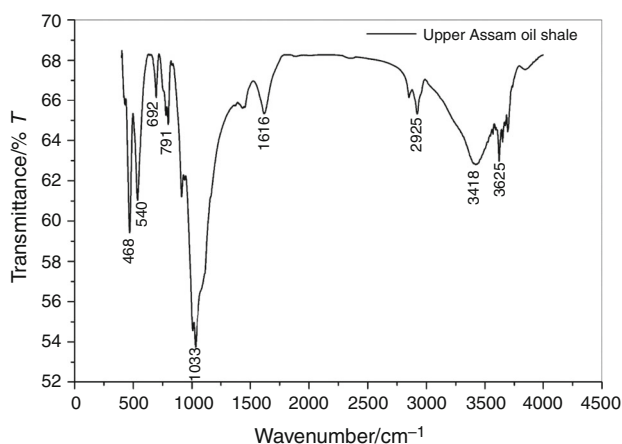
Fig. 1 FTIR spectra of Upper Assam oil shale

$$\ln\left(\frac{\beta_i}{T_{\alpha,i}^B}\right) = \text{constant} - C\left(\frac{E_a}{RT_\alpha}\right) \quad (2)$$

The approximations used in the formulation of the models are summarized in Table 1.

By following model-free isoconversional methods, the values of effective activation energy with conversion can be determined.

Determination of reaction model by Criado master plot

After determination of the apparent activation energies for constant values of conversion, the model of the reaction can be determined with the help of Criado master plot [38–42]. Criado master plot compares the experimental results with existing reaction models to predict the reaction model followed by the experimental decomposition results obtained from TG analysis. In this study, differential–integral Criado master plot or Z-alpha master plot has been used [38]. The generalized equation for Criado master plot is presented as follows [41, 42]:

$$\left(\frac{T}{T_{0.5}}\right)^2 \times \left(\frac{\theta\left(\frac{d\alpha}{d\theta}\right)}{\theta_{0.5}\left(\frac{d\alpha}{d\theta}\right)_{0.5}}\right) = \frac{[f(\alpha)g(\alpha)]}{[f(0.5)g(0.5)]} = \left(\frac{Z(\alpha)}{Z(0.5)}\right) \quad (3)$$

where $T_{0.5}$ and $\left(\frac{d\alpha}{d\theta}\right)_{0.5}$ represents the temperature and rate at $\alpha = 0.5$. The purpose of considering the above notations at $\alpha = 0.5$ as the reference point is to normalize the z(i) function [39].

The algebraic expressions of $f(\alpha)$ and $g(\alpha)$ for considered the theoretical reaction models are given in Table S1. The point $\alpha = 0.5$ is considered as the reference point because at $\alpha = 0.5$ the standard master plots of each considered kinetic mechanism intersect each other corresponding to value of $(d\alpha/d\theta)/(d\alpha/d\theta)_{0.5} = 1$ [38].

Table 3 Different functional groups detected by FTIR analysis of the Upper Assam oil shale

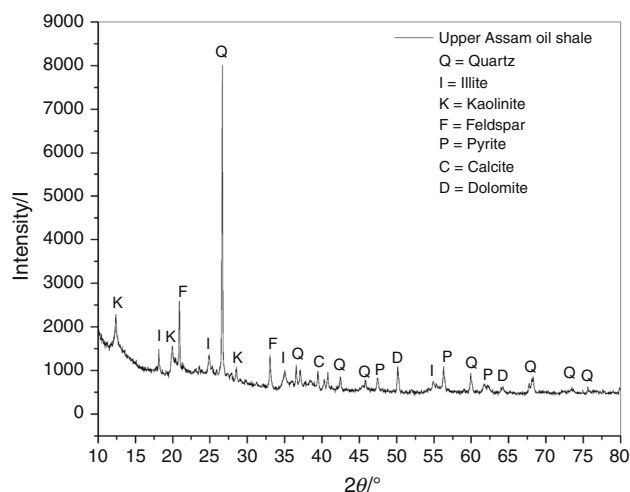| Wave numbers/cm^{-1}	Functional groups
3625	–OH group; alcohols and phenols (strong; sharp)
3300–3500	–OH stretch from –COOH and –COH
3000–2500	C–H stretch; alkanes; carboxylic acid stretch
1600–1650	Aromatic –C = O vibration; –C = O stretch from H-bonded conjugate
1020–1100	Silicate impurities; quartz
860–680	Aromatic C–H stretch;
680–610	S–O bending; sulfates

Fig. 2 XRD spectra of Upper Assam oil shale with determination of minerals

Table 4 XRD spectra analysis of oil shale

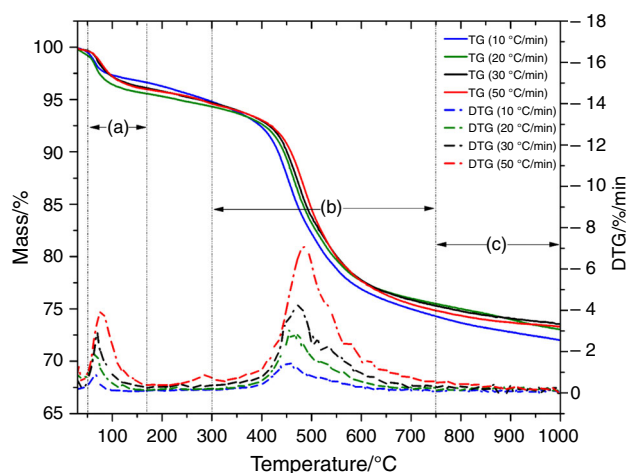| Minerals	Formula	Type	Percentage
Quartz	SiO_2	Siliceous	46.30
Illite	$(K,H_3O)(Al,Mg,Fe)_2$ $(Si,Al)_4O_{10}[(OH_2),H_2O]$	Siliceous (clay)	21.30
Kaolinite	$Al_2O_5Si_2(OH)_4$	Siliceous	15.40
Feldspar	$Al_2O_8Si_2Sr$	Siliceous	9.30
Pyrite	FeS_2	Sulfur	5.20
Calcite	$CaCO_3$	Carbonate	1.30
Dolomite	C_2CaMgO_6	Carbonate	1.10

Fig. 3 TG–DTG curves of Upper Assam oil shale at different heating rates of 10, 20, 30 and 50 °Cmin^{-1} from 30 to 1000 °C and differentiating **a** moisture loss, **b** organic decomposition, **c** mineral matter decomposition

Determination of pre-exponential factor using compensation factor

From the activation energy and the determined reaction model, the pre-exponential factor was determined using the compensation factor method [32, 33, 43]. The equation of compensation factor is given as:

$$\ln(A(f(\alpha))_\alpha = \frac{E_\alpha}{RT_\alpha} + \ln\left(\left(\frac{d\alpha}{dt}\right)_\alpha\right) \tag{4}$$

The equation can be simplified as:

$$b = \ln(A(f(\alpha))_\alpha - a \tag{5}$$

where $a = \frac{E_\alpha}{RT_\alpha}$ and $b = \ln\left(\left(\frac{d\alpha}{dt}\right)_\alpha\right)$.

According to this method, the values of activation energy, E and $A(f(\alpha))$ at various extents of conversion follow a logarithmic pattern and compensate one another in every stage of conversion. For each value of α, the values of a and b can be calculated. The values of $\ln(A(f(\alpha))_\alpha$ can be calculated from the intercept of the plot between b and a following isoconversional principle. Subsequently, using the model predicted by Criado master plot the values of pre-exponential factor can be determined using the term $\ln(A(f(\alpha))_\alpha$.

Reconstruction of kinetic data

The kinetic parameters obtained from different models were validated by subjecting to reconstruction of α vs T profiles. MATLAB 2016 was used for solving the differential equation, assuming temperature as an independent variable. The reconstruction methodology was used for each heating rate. The simulated data for α versus T profiles obtained from the reconstruction methodology were plotted against the experimental α versus T profiles, and the linearity of the fitting was verified by regression analysis.

Results and discussion

Characterization of oil shale

A comparison of Upper Assam oil shale with oil shales from different places around the world is summarized in Table 2. The ultimate and proximate analyses showed that oil shale sample obtained from Upper Assam, India, contains 30.06% carbon, high sulfur content of 3.61%, 31.78% volatile matter and ash content of 53.93%. The total organic carbon (TOC) was found to be 6.11% as calculated by the Walkley–Black titration method. The high sulfur percentage shows the oil shale to be sour in nature. The percentage of carbon in Indian oil shale was found to be

Table 5 The values of onset, offset and maximum decomposition temperatures for the pre-heating and organic matter decomposition

Heating rate/ °C min^{-1}	Pre-Heating (moisture loss)				Organic decomposition			
	Onset temperature/ °C	Maximum decomposition/°C	Offset temperature/ °C	Moisture loss/%	Onset temperature/ °C	Maximum decomposition/°C	Offset temperature/ °C	Mass loss/%
10	38.0	65.1	107.4	4	351.2	457.9	630.6	21
20	39.8	66.9	131.2	4	363.1	464.6	651.0	21
30	49.9	71.8	151.5	4	375.0	476.5	681.4	21
50	53.1	78.6	168.4	4	383.5	483.3	694.2	21

similar to Huadian and Gonglangtou oil shales of China [10, 44] and Kukersite oil shale of Estonia [45] and higher than most oil shales around the world such as Green River, Colorado, Israeli, Australian and Jordanian Oil shales [5, 19, 46, 47].

FTIR spectra obtained for oil shale sample are shown in Fig. 1, and the peaks identified are summarized in Table 3. FTIR analysis showed the presence of the alcohols, phenols, aliphatic, aromatic and sulfur stretching and bending overlapped with silica and clay mineral, such as quartz, kaolinite, illite and feldspar. The intensity of silica impurities was observed to be much higher. Hydroxyl group bands were observed from 3300 to 3500 cm^{-1}. A sharp peak corresponding to phenol and alcohol groups was observed at 3625 cm^{-1}. Presence of aliphatic compounds was observed at 2500–3000 cm^{-1} with a sharp peak at 2925 cm^{-1}. The aromatic bending was observed from 680 to 860 cm^{-1} with two sharp peaks at 692 cm^{-1} and 791 cm^{-1}. Silica impurities were observed from 1100 to 1020 cm^{-1} with a sharp peak at 1033 cm^{-1} depicting quartz.

The presence of minerals plays a significant role in the pyrolysis process. As reported in earlier works [14, 15], the presence of carbonate minerals restricts the emission of sulfur compounds and the silica compounds act as inhibitors to heat transfer during pyrolysis. XRD analysis (Fig. 2) showed the oil shale sample contains higher percentage of silica compounds and low percentage of calcite and dolomite (Table 4). Presence of pyrite was also detected which indicates the presence of inorganic sulfur. Higher percentage of silica compounds (92.30%) manifests that the Upper Assam oil shale can be classified as siliceous type. As the oil shale has low amount of carbonate minerals (1.30% calcite and 1.10% dolomite), it may promote emission of sulfur compounds during pyrolysis. The effect of higher percentage of silica can be observed in the higher activation energy as perceived from the kinetic study (Section "Kinetic Study").

Thermogravimetric analysis

TG was used to analyze the decomposition behavior of oil shale and studying the pyrolysis mechanism. Four different heating rates were considered at 10, 20, 30 and 50 °C min^{-1} (Fig. 3). The onset temperature at maximum decomposition temperature and the offset temperature corresponding to the pre-heating and organic decomposition region for each of the heating rate are given in Table 5. The TG curves showed that moisture loss (4%) in the pre-heating zone occurs from 35 to 170 °C. Significant decomposition corresponding to organic matter content (21%) was observed from 300 to 700 °C due to decomposition of the organic matter present in oil shale. Mineral matter decomposition has been reported to occur from 600 to 800 °C primarily due to decomposition of carbonate minerals [14, 15]. From 700 to 1000 °C, a continuous mass loss was observed. But, as observed in the TG plot, there was no notable occurrence of mineral matter decomposition, as the dominant minerals present in the oil shale sample were silica compounds, and silica compounds generally start degradation above 1200 °C. Minute amount of carbonate minerals (2.4%) was detected by XRD analysis. The continuous slope in the range of 700–1000 °C may have occurred because of decomposition of clay minerals such as illite and kaolinite and the minute amount of carbonate minerals.

Kinetic Study

TG data at four heating rates for the organic decomposition region were used to estimate the kinetic parameters by model-free isoconversional methods. The organic decomposition region was determined from the DTG curve (Fig. 3), by identifying the onset temperature (300 °C) and the offset temperature (700 °C). Model-free isoconversional method has been used to determine the kinetic parameters without the assumption of any kinetic model. The apparent activation energies obtained from the methods considered are shown in Fig. 4. The activation energy
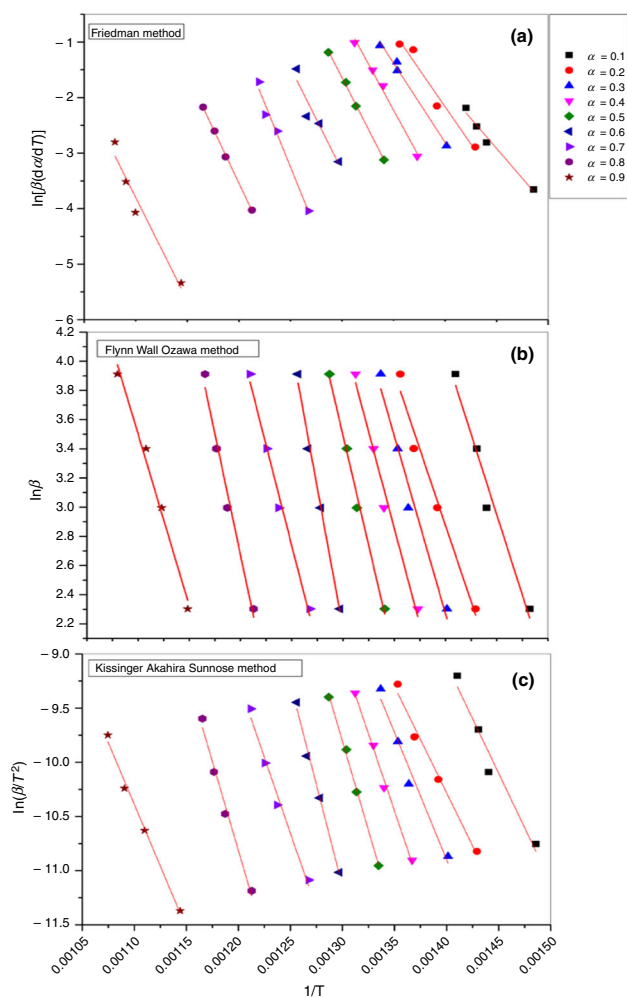
Fig. 4 R-squared correlation for determination of activation energy by **a** Friedman, **b** KAS and **c** FWO methods

Fig. 5 Distribution of activation energy obtained from Friedman, FWO and KAS methods

was determined by both differential and integral methods, viz. Friedman method (differential) and FWO and KAS methods (integral). The correlation of the activation energies for each method at each conversion from $\alpha = 0.1$ to 0.9 is shown in Fig. 5. Friedman method showed a mean activation energy of 249.75 kJmol^{-1}, whereas FWO and KAS showed mean activation energies of 241.20 kJmol^{-1} and 239.68 kJmol^{-1}, respectively. The activation energies obtained for the Upper Assam oil shale were observed to be similar to those reported for Huadian oil shale [48], Green River oil shale [17], Moroccan oil shale [24, 49] and Kukersite oil shale [50]. This is because of the presence of higher percentage of silica compounds which act as inhibitors for heat transfer, leading to higher consumption of energy.

The derived activation energy was later used to determine the kinetic model and the pre-exponential factor. The kinetic model for the pyrolysis process was determined by
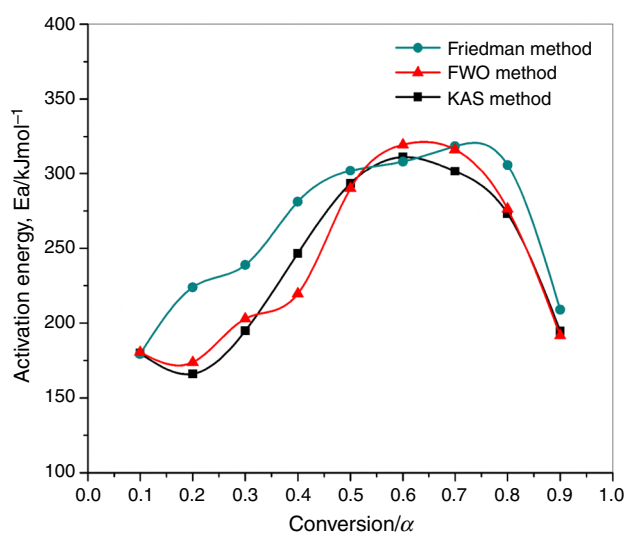
applying the differential–integral $\left(\frac{Z(\alpha)}{Z(0.5)}\right)$ Criado master plot [38]. For determining the reaction mechanism or kinetic model, the activation energy at $\alpha = 0.5$ for each method has been considered. The standard master plots were formed (Eq. 4), and the plot for the experimental pyrolysis mechanism was plotted. The resultant plot shows the decomposition of oil shale follows D3 diffusion mechanism till $\alpha = 0.8$ and fall upon A2 Avrami Erofeev mechanism at $\alpha = 0.9$. Previous works on oil shale kinetics have shown the event of multiple reactions during oil shale pyrolysis [17, 21]. These multiple reactions may suggest the occurrence of heat diffusion, mass diffusion, nucleation growth and other subsequent reactions. The manifestation of the D3 diffusion mechanism might be because of the diffusion of heat and mass through the pores of oil shale. The heat diffusion may occur due to the conductive heat transfer from the reactor to oil shale and from the mineral matrix to the kerogen mass and from the converted kerogen to the unconverted kerogen by both conductive and convective modes of heat transfer. The mass transfer corresponds to the diffusion of the liquid and gaseous products through the pores of oil shale after conversion of the kerogen and bitumen. The A2 Avrami Erofeev model observed at $\alpha = 0.9$ may justify the coking of the oil products which is caused by the secondary coking reactions predicted to occur during oil shale pyrolysis. The A2 Avrami Erofeev model was observed for the activation energies considered from each method. KAS method showed higher co-relation factor for the experimental $f(\alpha)$ versus theoretical $f(\alpha)$ ($R^2 = 0.988$). Criado master plot using the values of activation energy obtained by the KAS
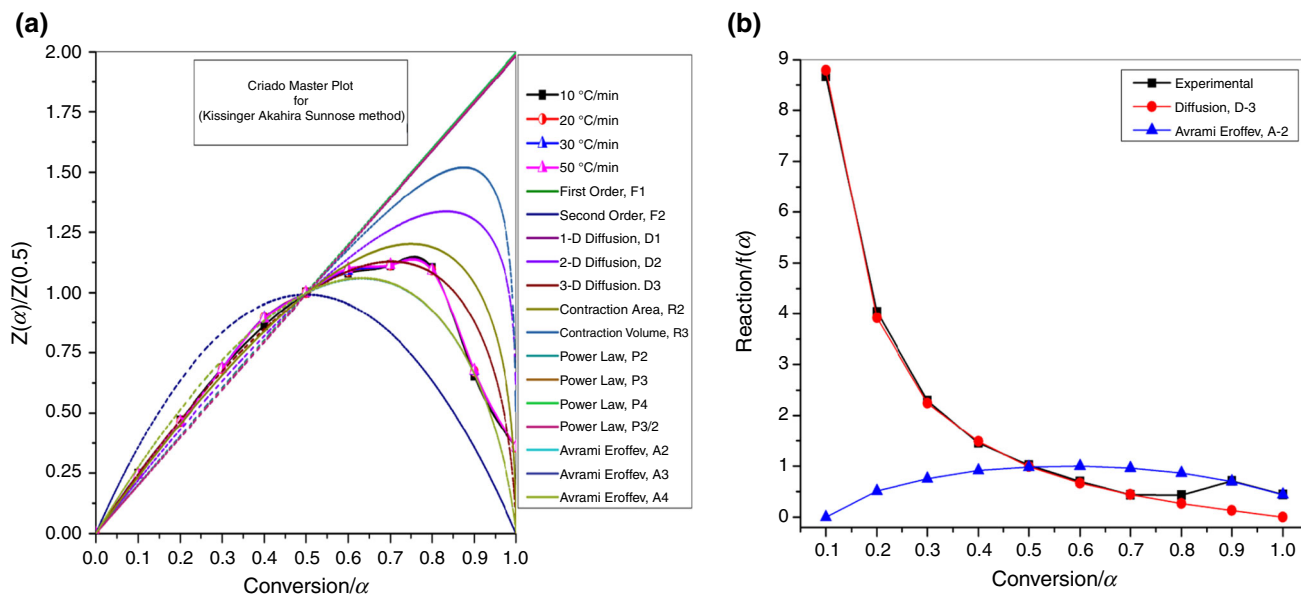
Fig. 6 **a** Criado master plot for KAS method; **b** experimental $f(\alpha)$ and theoretical $f(\alpha)$ plot

Table 6 Effective activation energy values estimated using Friedman, FWO and KAS methods for constant values of α

Conversion, α	Friedman method			FWO method			KAS method			Reaction model, $f(\alpha)$
	Activation energy, Ea/ kJ mol^{-1}	R^2	Pre-Exponential factor, A/s^{-1}	Activation energy, Ea/ kJ mol^{-1}	R^2	Pre-exponential factor, A/s^{-1}	Activation energy, Ea/ kJ mol^{-1}	R^2	Pre-exponential factor, A/s^{-1}	
0.1	179.29	0.9887	4.96×10^{12}	180.59	0.9648	4.83×10^{12}	179.82	0.9969	4.81×10^{12}	D3
0.2	223.91	0.9665	6.57×10^{15}	173.82	0.9861	5.31×10^{15}	162.81	0.9948	5.17×10^{15}	D3
0.3	238.80	0.9775	4.67×10^{16}	202.89	0.9782	4.17×10^{16}	194.81	0.9891	4.02×10^{16}	D3
0.4	281.04	0.9932	1.91×10^{19}	219.61	0.9893	1.29×10^{19}	246.60	0.9974	1.91×10^{19}	D3
0.5	301.91	0.9618	1.49×10^{20}	290.05	0.9914	1.31×10^{20}	293.35	0.9983	1.50×10^{20}	D3
0.6	308.25	0.9572	7.55×10^{19}	319.49	0.9963	7.13×10^{19}	311.20	0.9969	7.15×10^{19}	D3
0.7	318.40	0.9879	1.55×10^{19}	316.22	0.9867	1.53×10^{19}	301.57	0.9942	1.24×10^{19}	D3
0.8	305.93	0.9943	1.89×10^{16}	276.28	0.9780	1.60×10^{16}	273.08	0.9903	1.59×10^{16}	D3
0.9	208.87	0.9546	3.022×10^{16}	191.80	0.9851	2.93×10^{16}	194.69	0.9871	2.93×10^{16}	A2

Table 7 Comparison of kinetic triplets of Indian oil shale with other oil shales

| Oil shales	Mean activation energy of organic decomposition zone Ea/kJ mol^{-1}	Mean pre-exponential factor A/s^{-1}	Reaction models, $f(\alpha)$
Upper Assam[a]	247.56	2.56×10^{19}	D3 and A2
Green River [17]	168.50	2.23×10^{16}	First order
Kukersite [50]	235	1×10^{13}	Discrete distribution and third order
Huadian [44]	230	1.87×10^{27}	D1 and A5/6
Moroccan [49]	270.23	4.24×10^{17}	nth and pseudo-first order, $n = 1.67$

[a]Tikak Colliery, Makum Coal Field, Margherita, Upper Assam, India
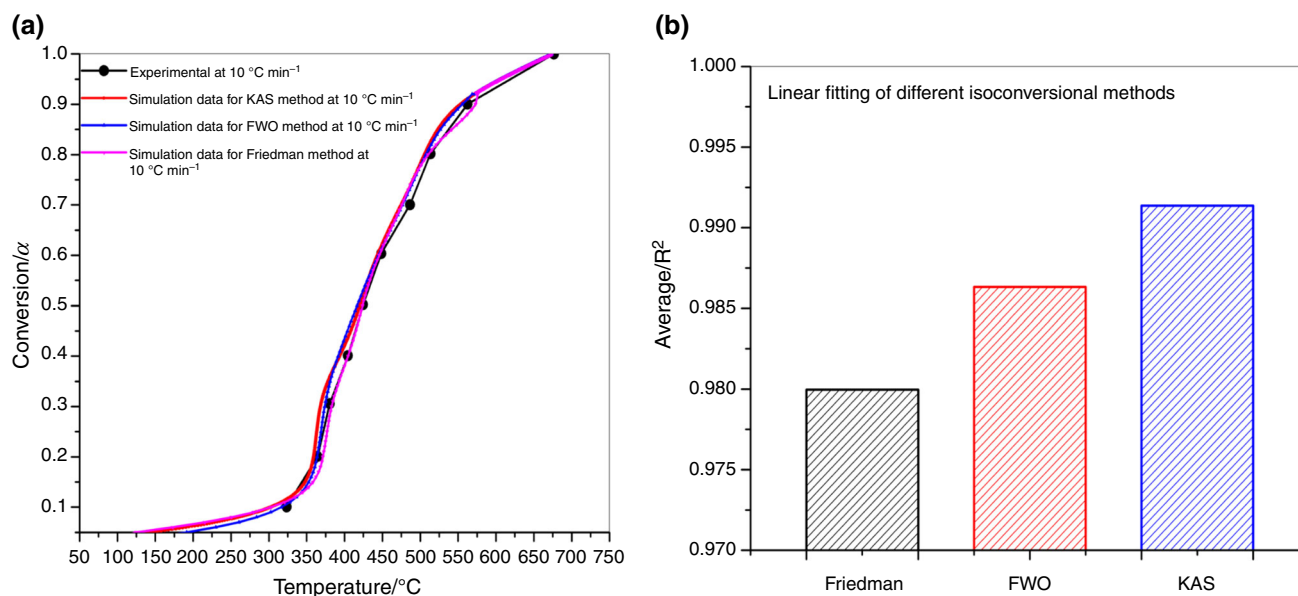
Fig. 7 **a** Experimental and simulation (KAS, FWO and Friedman methods) conversion profile at heating rate of 10 °C min^{-1}. **b** Comparison of different isoconversional methods based on linear average coefficient (i^2) between experimental and reconstruction profile

method is shown in Fig. 6a. The Criado master plots for Friedman method and FWO method are shown in Supplementary Figs. S1 and S2, respectively.

The compensation factor method was applied for the models obtained from Criado master plot. The reaction order showed a high regression coefficient for D3 and A2 Avrami Erofeev model at different levels of conversion. These compensation parameters were used to evaluate the pre-exponential factor, A, at different conversions. The average value obtained is 2.56×10^{19} s^{-1} for KAS method. The experimental $f(\alpha)$ values for each method were determined using E and A values and compared with the theoretical $f(\alpha)$ values. The comparison for values obtained for KAS model is shown in (Fig. 6b). The variations in kinetic parameters with progress of decomposition uphold the multimodel process; D3 model up to $\alpha = 0.8$ and A2 Avrami Erofeev model at $\alpha = 0.9$. The effective activation energies, the pre-exponential factors and reaction model are listed in Table 6. The kinetic parameters obtained are in the ranges of reported values in the literature (Table 7).

The reconstruction of kinetic data showed the validation of similarity between the experimental profiles and the simulated profiles. The simulated and experimental data profiles for Friedman, FWO and KAS methods with respect to experimental data at heating rate of 10 °C min^{-1} are shown in Fig. 7a. Regression analysis for linearity fitting was performed for each heating rate (10, 20, 30 and 50 °C min^{-1}), and the average linearity fitting coefficient (R^2) corresponding to each method is shown in Fig. 7b.

KAS model to possess highest average R^2 value of 0.9923. FWO showed average R^2 of 0.9863, and Friedman method showed the lowest value of 0.9799. Over the R^2 average value, KAS model is considered to be the most appropriate for studying the kinetics of thermal degradation for the Indian oil shale. The simulated vs experimental profiles for KAS method for each heating rate are shown in Fig. 8. The profiles for Friedman and FWO methods at each heating rate are shown in Figs. S3 and S4 in supplementary data.

Conclusions

The physicochemical analysis showed Upper Assam oil shale to be siliceous in nature. Presence of minute amount of carbonate minerals in the oil shale was shown by XRD analysis and TG–DTG curve for mineral matter decomposition. The presence of higher percentage of sulfur, pyrite and sulfur oxide compounds detected by CHNS, XRD and FTIR shows the oil shale to be sour. The organic matter content was found to be about 21 mass%. The physical characteristics of the oil shale were found to be similar to the Kukersite oil shale of Estonia. The kinetic study reported in this paper is first of its kind for Upper Assam oil shale. The study exhibited an average activation energy of 247.56 kJmol^{-1}, which was in range with the benchmark oil shales such as Green River, Kukersite, Huadian, Sultani and Queensland. The activation energy appeared to be low during the initial stage of degradation, corresponding to moisture loss and onset of organic
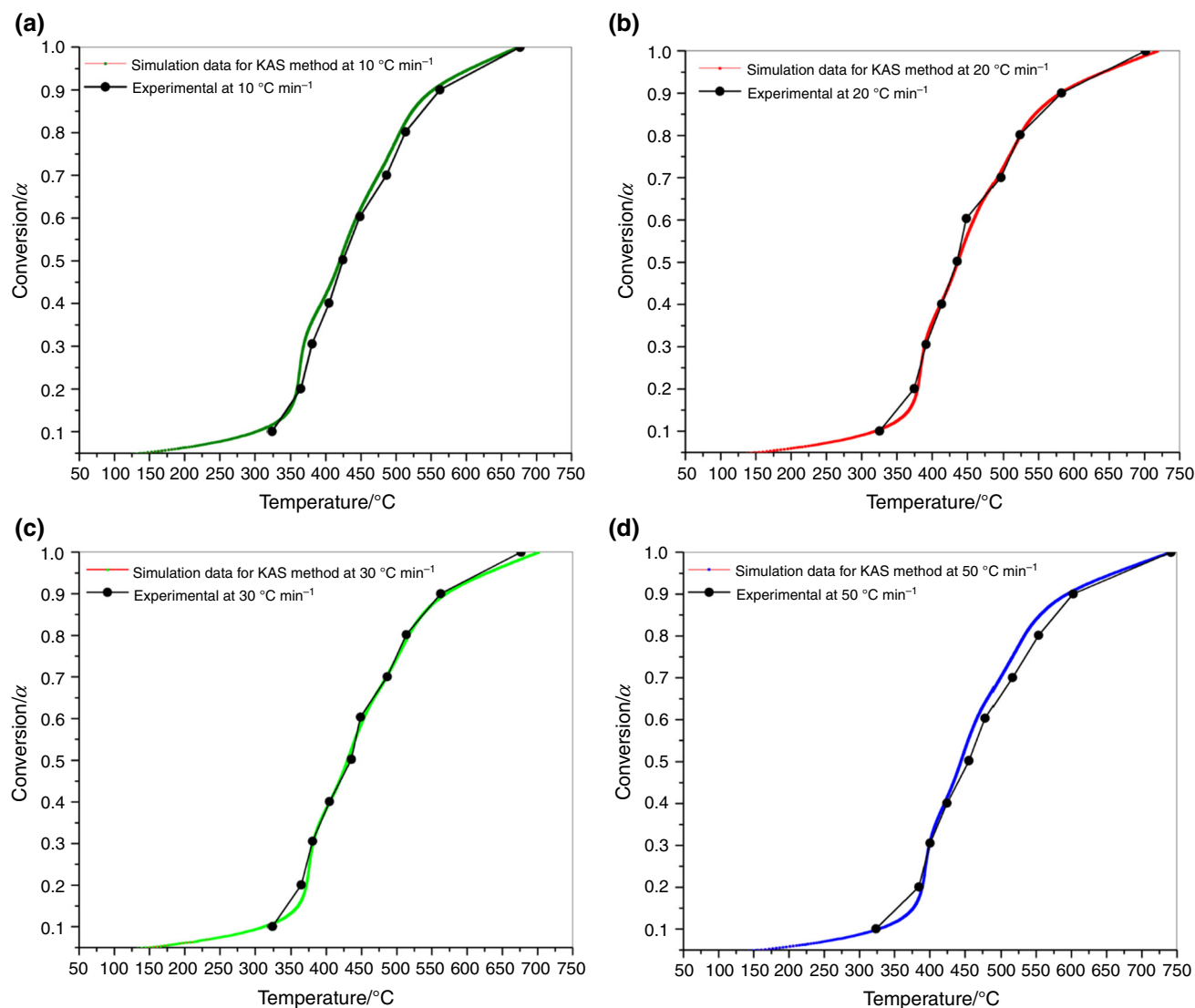
(a)

(b)

(c)

(d)

Fig. 8 Fitness of experimental to simulated profile for KAS method at heating rate of **a** 10, **b** 20, **c** 30, **d** 50 °C min^{-1}

decomposition. The subsequent increase in activation energy corresponds to the degradation of the heavier hydrocarbon molecules. The reaction kinetics follows two models, viz. D3 diffusion model followed by Avrami Erofeev which corresponds to the heat and mass diffusion during thermal degradation of the oil shale and secondary coking reactions. The change in activation energy with respect to conversion, and the shift of reaction mechanism during degradation reflects the complex nature of oil shale pyrolysis.

References

1. Gwyn JE. Oil from shale as a viable replacement of depleted crude reserves: processes and challenges. Fuel Process Technol. 2001;70:27–40.
2. Tiwari P. Oil shale pyrolysis: benchscale experimental studies and modelling. Utah: University of Utah; 2012.
3. Braun RL, Rothman AJ. Oil shale pyrolysis: kinetics and mechanism of oil production. Fuel. 1975;54(April):129–31.
4. Charlesworth JM. Oil shale pyrolysis: 1. Time and temperature dependance of product composition. Ind Eng Chem Process Des Dev. 1985;24:1117–25.
5. Solomon PR, Carengelo RM, Horn E. The effect of pyrolysis conditions on Israeli oil shale particles. Fuel. 1986;65(May):650–62.
6. Li S, Qian J. Study of the pyrolysis of Maoming oil shale lumps. Fuel. 1991;70:1371–5.
7. Stirzhakova YA, Usova TV. Current trends in pyrolysis of oil shale: a review. Solid Fuel Chem. 2008;42(4):197–201.

8. Ren L, Xia D, Xu Y, Guo M, Sun H, Liu X. Research on pyrolysis mechanism of Huadian oil shale. Energy Procedia. 2015;66:13–6. https://doi.org/10.1016/j.egypro.2015.02.007.

9. Nazzal JM. Influence of heating rate on the pyrolysis of Jordanian oil shale. J Anal Appl Pyrol. 2002;62:225–38.

10. Han X, Liu Q, Jiang X. Heat transfer characteristics of oil shale particle during the retorting. Int J Heat Mass Transf. 2015;84:578–83.

11. Kumar R, Bansal V, Badhe RM, Madhira ISS, Sugumaran V, Ahmed S, et al. Characterization of Indian origin oil shale using advanced analytical techniques. Fuel. 2013;113:610–6. https://doi.org/10.1016/j.fuel.2013.05.055.

12. Hutton AC. Petrographic classification of oil shale. Int J Coal Geol. 1987;8:203–31.

13. Cook AC, Sherwood NR. Clasification of oil shales, coal and other organic rocks. Org Geochem. 1991;17(2):211–22.

14. Patterson JH. A review on the effects of minerals in processing of Australian oil shales. Fuel. 1994;73(3):321–7.

15. Patterson JH, Hurst HJ, Levy JH, Killingley JS. Mineral reactions in the processing of Australian Tertiary oil shales. Fuel. 1990;69(September):1119–23.

16. Patterson JH, Hurst HJ, Levy JH. Relevance of carbonate minerals in the processing of Australian Tertiary oil shales. Fuel. 1991;70(November):1252–9.

17. Tiwari P, Deo M. Detailed kinetic analysis of oil shale using TGA data. AIChE. 2012;58(2):505–16. https://doi.org/10.1002/aic.12589.

18. Bai F, Sun Y, Liu Y, Li Q, Guo M. Thermal and kinetic characteristics of pyrolysis and combustion of three oil shales. Energy Convers Manag. 2015;97:374–81.

19. Jaber JO, Probert SD. Non-isothermal thermogravimetry and decomposition kinetics of two Jordanian oil shales under different processing conditions. Fuel Process Technol. 2000;63:57–70.

20. Ekstrom A, Callaghan G. The pyrolysis kinetics of some Australian oil shales. Fuel. 1987;66(March):331–7.

21. Skala D, Kopsch H, Sokic M, Neumann HJ, Jovanovic J. Modelling and simulation of oil shale pyrolysis. Fuel. 1989;68(February):168–73.

22. Han H, Nn Zhong, Cx Huang, Zhang W. Pyrolysis kinetics of oil shale from northeast China: implications from thermogravimetric and Rock-Eval experiments. Fuel. 2015;157:776–83. https://doi.org/10.1016/j.fuel.2015.07.052.

23. Braun RL, Burnham AK. Kinetics of Colorado oil shale pyrolysis in a fluidized-bed reactor. Fuel. 1986;65:218–22.

24. Aboulkas A, Harfi KE. Study of the kinetics and mechanisms of thermal decomposition of Moroccan Tarfaya oil shale and its kerogen. Oil Shales. 2008;25(4):426–43. https://doi.org/10.3176/oil.2008.4.04.

25. Harahsheh MA, Ayed OA, Robinson J, Kingman S, Harahsheh AA, Tarawneh K, et al. Effect of demineralization and heating rate on the pyrolysis kinetics of Jordanian oil shales. Fuel Process Technol. 2011;92:1805–11. https://doi.org/10.1016/j.fuproc.2011.04.037.

26. Vyazovkin S, Wight CA. Model free and model fitting approaches to kinetic analysis of isothermal and non-isothermal data. Thermochim Acta. 1999;340–341:53–68.

27. Youhong S, Shuai Z, Qiang L, Shichang L, Jing H. Thermoelectric coupling analysis of high-voltage breakdown industrial frequency pyrolysis in Fuyu oil shale. Int J Therm Sci. 2018;130:19–27. https://doi.org/10.1016/j.ijthermalsci.2018.03.013.

28. Sańchez-Jimeńez PE, Perez-Maqueda LA, Perejón A, Criado JM. Generalized kinetic master plots for the thermal degradation of polymers following a random scission mechanism. J Phys Chem A. 2010;114:7868–76.

29. Gelman F, Binstock R, Halicz L. Application of the Walkley–Black titration for the organic carbon quantification in organic rich sedimentary rocks. Fuel. 2012;96:608–10. https://doi.org/10.1016/j.fuel.2011.12.053.

30. Torrente MC, Galan MA. Kinetics of the thermal decomposition of oil shale from Puertollano (Spain). Fuel. 2001;80:327–34.

31. Li S, Yue C. Study of different kinetic models for oil shale pyrolysis. Fuel Process Technol. 2003;85:51–61. https://doi.org/10.1016/S0378-3820(03)00097-3.

32. Vyazovkin S. Model free kinetics, staying free of multiplying entities without necessity. J Therm Anal Calorim. 2006;83(1):45–51.

33. Vyazovkin S, Burnham AK, Criado JM, Parez-Maqueda LA, Popescu C, Sbirrazzuoli N. ICTAC kinetic committee recommendations for performing kinetic computations on thermal analysis data. Thermochim Acta. 2011;520:1–19.

34. Al-makhadmeh LA, Maier J, Batiha MA, Scheffknecht G. Oxy-fuel technology: oil shale desulfurization behavior during staged combustion. Fuel. 2017;190:229–36. https://doi.org/10.1016/j.fuel.2016.11.022.

35. Yu X, Luo Z, Li H, Gan D. Effect of vibration on the separation efficiency of oil shale in a compound dry separator. Fuel. 2018;214:242–53. https://doi.org/10.1016/j.fuel.2017.10.129.

36. Maes J, Muggeridge AH, Jackson MD, Quintard M, Lapene A. Scaling analysis of the In-Situ upgrading of heavy oil and oil shale. Fuel. 2017;195:299–313. https://doi.org/10.1016/j.fuel.2017.01.072.

37. Wang Q, Hou Y, Wu W, Liu Q, Liu Z. The structural characteristics of kerogens in oil shale with different density grades. Fuel. 2018;219:151–8. https://doi.org/10.1016/j.fuel.2018.01.079.

38. Gotor FJ, Criado JM, Malek J, Koga N. Kinetic analysis of solid-state reactions: the universality of master plots for analyzing isothermal and nonisothermal experiments. J Phys Chem. 2000;104:10777–82.

39. Criado JM. Kinetic analysis of DTG data from master curve. Thermochim Acta. 1978;24:186–9.

40. Criado JM, Malek J, Ortega A. Applicability of the master plots in kinetic analysis of non-isothermal data. Thermochim Acta. 1989;147:377–85.

41. Sánchez-Jiménez PE, Pérez-Maqueda LA, Perejón A, Criado JM. Generalized master plots as a straightforward approach for determining the kinetic model: the case of cellulose pyrolysis. Thermochim Acta. 2013;552:54–9. https://doi.org/10.1016/j.tca.2012.11.003.

42. Sánchez-Jiménez PE, Pérez-Maqueda LA, Perejón A, Criado JM. A new model for the kinetic analysis of thermal degradation of polymers driven by random scission. Polym Degrad Stab. 2010;95(5):733–9. https://doi.org/10.1016/j.polymdegradstab.2010.02.017.

43. Vyazovkin S, Wight CA. Isothermal and non-isothermal kinetics of thermally simulated reactions of solid. Int Rev Phys Chem. 1998;17(3):407–33.

44. Bai F, Guo W, Lu X, Liu Y, Guo M, Li Q, et al. Kinetic study on the pyrolysis behaviour of Huadian oil shale via non isothermal thermogravimetric data. Fuel. 2015;146:111–8. https://doi.org/10.1016/j.fuel.2014.12.073.

45. Loo L, Maaten B, Siirde A, Pihu T, Konist A. Experimental analysis of the combustion characteristics of Estonian oil shale in air and oxy-fuel atmospheres. Fuel Process Technol. 2015;134:317–24. https://doi.org/10.1016/j.fuproc.2014.12.051.

46. Tiwari P, Deo M. Compositional and kinetic analysis of oil shale pyrolysis using TGA-MS. Fuel. 2012;94:333–41. https://doi.org/10.1016/j.fuel.2011.09.018.

47. Amer MW, Marshall M, Fei Y, Jackson WR, Gorbaty ML, Cassidy PJ, et al. The structure and reactivity of a low-sulfur lacustrine oil shale (Colorado U.S.A.) compared with those of a

high-sulfur marine oil shale (Julia Creek, Queensland, Australia). Fuel Process Technol. 2015;135:91–8. https://doi.org/10.1016/j.fuproc.2014.10.032.

48. Wang Z, Deng S, Gu Q, Zhang Y, Cui X, Wang H. Pyrolysis kinetic study of Huadian oil shale, spent oil shale and their mixtures by thermogravimetric analysis. Fuel Process Technol. 2013;110:103–8. https://doi.org/10.1016/j.fuproc.2012.12.001.

49. Ec Moine, Groune K, El Hamidi A, Khachani M, Halim M, Arsalane S. Multistep process kinetics of the non-isothermal pyrolysis of Moroccan Rif oil shale. Energy. 2016;115:931–41. https://doi.org/10.1016/j.energy.2016.09.033.

50. El Nady MM, Hammad MM. Organic richness, kerogen types and maturity in the shales of the Dakhla and Duwi formations in Abu Tartur area, Western Desert, Egypt: implication of Rock-Eval pyrolysis. Egypt J Pet. 2015;24(4):423–8. https://doi.org/10.1016/j.ejpe.2015.10.003.

51. Gerasimov G, Khaskhachikh V, Potapov O. Experimental study of kukersite oil shale pyrolysis by solid heat carrier. Fuel Process Technol. 2017;158:123–9. https://doi.org/10.1016/j.fuproc.2016.12.016.

52. Lewan MD, Roy S. Role of water in hydrocarbon generation from Type-I kerogen in Mahogany oil shale of the Green River Formation. Org Geochem. 2011;42(1):31–41. https://doi.org/10.1016/j.orggeochem.2010.10.004.

53. Maaten B, Loo L, Konist A, Pihu T, Siirde A. Investigation of the evolution of sulphur during the thermal degradation of different oil shales. J Anal Appl Pyrolysis. 2017;128:405–11. https://doi.org/10.1016/j.jaap.2017.09.007.

54. Gregg ML, Campbell JH, Taylor JR. Laboratory and modelling investigation of a Colorado oil shale block heated at 900°C. Fuel. 1981;60(March):179–88.

55. Xu J, Meng Q, Li B, Liu R, Xu Y, Gratzer R, et al. Oil yield and bulk geochemical parameters of oil shales from the Songliao and Huadian Basins, China: a grade classification approach. Oil Shale. 2013;30(3):402. https://doi.org/10.3176/oil.2013.3.03.